Near Doping-Independent Pocket Area from an Antinodal Fermi Surface Instability in Underdoped High Temperature Superconductors

N. Harrison

Los Alamos National Laboratory, MS E536, Los Alamos, New Mexico 87545, USA

(Received 8 August 2011; published 28 October 2011)

Fermi surface models applied to the underdoped cuprates predict the small pocket area to be strongly dependent on doping whereas quantum oscillations in $YBa_2Cu_3O_{6+x}$ find precisely the opposite to be true—seemingly at odds with the Luttinger volume. We show that such behavior can be explained by an incommensurate antinodal Fermi surface nesting-type instability—further explaining the doping-dependent superstructures seen in cuprates using scanning tunneling microscopy. We develop a Fermi surface reconstruction scheme involving orthogonal density waves in two dimensions and show that their incommensurate behavior requires momentum-dependent coupling. A cooperative modulation of the charge and bond strength is therefore suggested.

DOI: 10.1103/PhysRevLett.107.186408 PACS numbers: 71.18.+y, 71.45.Lr, 74.72.−h, 75.40.Mg

Identification of the forms of order competing with superconductivity and antiferromagnetism in the high-T_c cuprates remains a considerable experimental challenge [1,2]. Among possibilities, charge ordering is reported in several experiments within the underdoped regime—namely x-ray diffraction [3,4], neutron scattering [4], scanning tunneling microscopy (STM) [5] and nuclear magnetic resonance (NMR) [6] [see Fig. 1(a)]. Yet its extent and relevance are far from understood. It is yet to be established whether such ordering participates in forming the pseudogap [5], whether it is inherently unidirectional as opposed to bidirectional in nature [7], or whether it is caused by a Fermi surface instability [8] as opposed to being a biproduct of spin order [4].

In the light of recent quantum oscillation [9,10], electrical transport [11] and angle-resolved photoemission spectroscopy (ARPES) [12] studies, several Fermi surface reconstruction models have been invoked in the underdoped cuprates postulating charge (and/or other forms of) ordering [10,13–15]. A serious problem with *all* proposed models, however, is that they predict the pocket size to be strongly dependent on the hole doping [e.g., dotted and dashed lines in Fig. 1(b)], whereas experiments on underdoped $YBa_2Cu_3O_{6+x}$ [16–19] find the pocket area to change remarkably little over a range of hole dopings spanning $\approx 3\%$ [20] [circles in Fig. 1(b)].

In this Letter, we show that the near doping-independence of the orbit area in underdoped $YBa_2Cu_3O_{6+x}$ [16,17,20] and the increasing charge modulation period seen with hole doping in STM experiments on $Bi_{2-y}Pb_ySr_{2-z}La_zCuO_{6+x}$ [8] can both be consistently explained by Fermi surface reconstruction resulting from an antinodal Fermi surface nesting-type instability [i.e., at $[\pm\frac{\pi}{a}, 0]$ and $[0, \pm\frac{\pi}{b}]$ in Fig. 2(a)]. We present a density-wave model in which we mimic incommensurate behavior by considering modulation periods λ corresponding to different rational multiples of the in plane lattice vectors (e.g., $\lambda = 7/2, 4, 13/3, 9/2, 5$, 6, and 7). On treating scenarios in which the coupling between translated bands is uniform (as in a charge-density wave [13,15]) or acquires a momentum dependence (as occurs on incorporating a bond-density-wave component [22]), we find that only the latter leads to a single well-defined gap in the electronic density-of-states at weak couplings $V_{x,y} \ll t_{10}$ (where t_{10} is the nearest neighbor hopping [23]). We show the latter also to be a necessary prerequisite for incommensurate behavior, in which the electronic structure evolves continuously as a function of λ.

We model Fermi surface reconstruction caused by modulations of general period $\lambda = n/m$ (in which n and m are integers) along the a and/or b lattice directions by diagonalizing a Hamiltonian consisting of nested matrices

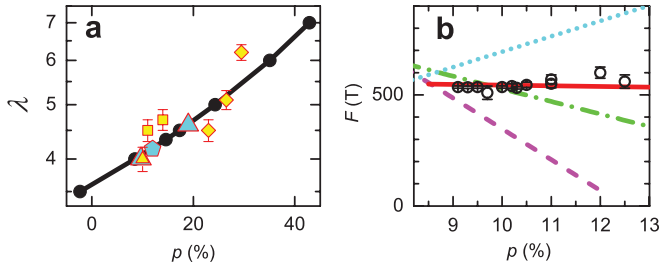

FIG. 1 (color online). (a) Charge modulation periods seen using x-rays or NMR in $YBa_2Cu_3O_{6+x}$ [3,6] (large triangles), $La_{1.875}Ba_{0.125}CuO_4$ and $La_{1.48}Nd_{0.4}Sr_{0.12}CuO_4$ [4] (pentagon) and STM in $Bi_{2-y}Pb_ySr_{2-z}La_zCuO_{6+x}$ (diamonds), $Bi_2Sr_2CaCu_2O_{8+\delta}$ (squares) and $Ca_{2-x}Na_xCuO_2Cl_2$ (small triangle) taken from Ref. [8]. In comparing different materials, we neglect possible differences in $\varepsilon(\mathbf{k})$ [23]. The line and circles show the doping p for each λ extracted from the model density-of-states minimum [e.g., Fig. 3(b)]. (b) Measured leading $YBa_2Cu_3O_{6+x}$ quantum oscillation frequency [16–20] (circles) compared to its strong p dependence expected in the 4 hole pocket [1] (dotted line), Millis and Norman stripe [13] (dot-dash line) and fixed $\lambda = 4$ bidirectional charge [15] (dashed line) models, where $F = (\hbar/2\pi e)A_e$. The present model (solid line) uniquely yields a weakly p-dependent F [20].

$$\mathbf{H}_{xy} = \begin{pmatrix} \mathbf{H}_x(0) & V_y\mathbf{I}_n & 0 & \dots & 0 & V_y\mathbf{I}_n \\ V_y\mathbf{I}_n & \mathbf{H}_x(1) & V_y\mathbf{I}_n & \dots & 0 & 0 \\ 0 & V_y\mathbf{I}_n & \mathbf{H}_x(2) & \dots & 0 & 0 \\ \vdots & \vdots & \vdots & \ddots & \vdots & \vdots \\ 0 & 0 & 0 & \dots & \mathbf{H}_x(n'-2) & V_y\mathbf{I}_n \\ V_y\mathbf{I}_n & 0 & 0 & \dots & V_y\mathbf{I}_n & \mathbf{H}_x(n'-1) \end{pmatrix}. \quad (1)$$

Here, $\mathbf{I}_n$ is an identity matrix of rank n, $n' = n$ for bidirectional order (or $n' = 1$ for unidirectional order),

$$\mathbf{H}_x(i) = \begin{pmatrix} \varepsilon_{i\mathbf{Q}_y} & V_x & 0 & \dots & 0 & V_x \\ V_x & \varepsilon_{\mathbf{Q}_x+i\mathbf{Q}_y} & V_x & \dots & 0 & 0 \\ 0 & V_x & \varepsilon_{2\mathbf{Q}_x+i\mathbf{Q}_y} & \dots & 0 & 0 \\ \vdots & \vdots & \vdots & \ddots & \vdots & \vdots \\ 0 & 0 & 0 & \dots & \varepsilon_{(n-2)\mathbf{Q}_x+i\mathbf{Q}_y} & V_x \\ V_x & 0 & 0 & \dots & V_x & \varepsilon_{(n-1)\mathbf{Q}_x+i\mathbf{Q}_y} \end{pmatrix}$$

and $\varepsilon_{j\mathbf{Q}_x+i\mathbf{Q}_y}$ represents the electronic dispersion $\varepsilon(\mathbf{k})$ [23] subject to translation by multiples of $\mathbf{Q}_x = [\frac{2\pi}{\lambda a}, 0]$ and $\mathbf{Q}_y = [0, \frac{2\pi}{\lambda b}]$.

In the case of a conventional density wave, the normal assumption is for the potentials to uniformly couple all band crossings subject to a relative translation by $\mathbf{Q}_x$ or $\mathbf{Q}_y$ such that $V_x = V_{x,0}$ and $V_y = V_{y,0}$ are constants in Eq. (1). In the case of incommensurate ordering in a two-dimensional lattice, however, the coupling V has been found to vary depending on the band crossing in question [26,27]. Such behavior is most apparent in $R\mathrm{Te}_3$ [26] (owing to its exceptionally large gap), where ARPES finds a momentum-dependent $V(\mathbf{k})$ that selectively couples portions of the Fermi surface subject to nesting.

While the real-space implications of a momentum-dependent coupling in the chalcogenides has yet to be investigated, in the cuprates it is connected with the possibility of bond-strength or bond-current density-wave ordering [22]. We find a simple form of the coupling [28],

$$V_x(\mathbf{k}) = V_{x,0}\frac{1}{1-r}(1 - r\cos bk_y)$$
$$V_y(\mathbf{k}) = V_{y,0}\frac{1}{1-r}(1 - r\cos ak_x), \quad (2)$$

in which r adds a bond-strength modulation to an otherwise conventional charge-density wave, to prove particularly effective at reducing the electronic density-of states (and consequent free energy) when $r \approx 1$ [29]. It does so by suppressing $V(\mathbf{k})$ in the regions of the Brillouin zone where unnested bands cross [29], which we demonstrate in Fig. 2 by considering the simple case of a unidirectional modulation $\mathbf{Q}_x = [\frac{2\pi}{\lambda a}, 0]$ [in which $\lambda = 4$, $n = 4$ and $n' = 1$ in Eq. (1)].

From Figs. 2(b) and 2(c) it is evident that while both uniform ($r = 0$) and strongly momentum dependent ($r = 1$) forms of V_x open a gap at $|k_y| > \frac{\pi}{2b}$, where the Fermi surfaces are nested by $\mathbf{Q}_x$, the latter does so without splitting the open Fermi surfaces at $k_y \approx \pm\frac{\pi}{4b}$.

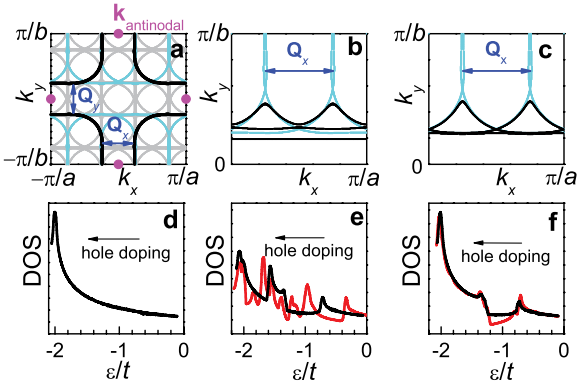

FIG. 2 (color online). (a) The unreconstructed Fermi surface at $p = 8.5\%$ (black) [23] together with itself translated by multiples of $\mathbf{Q}_x$ (cyan) and multiples of $\mathbf{Q}_x$ and $\mathbf{Q}_y$ (grey) for $\lambda = 4$. (b) Reconstructed Fermi surface (black) resulting from a unidirectional charge modulation (i.e., $n' = 1$) in which $V_{x,0} = 0.3t$ and $r = 0$ in Eq. (2), shown for a quadrant of the extended Brillouin zone. (c) Same as (b) but with a momentum-dependent V_x in which we choose $r = 1$ [29]. (d) The calculated electronic density-of-states (DOS) for the unreconstructed band [23] exhibiting a van Hove singularity near $\varepsilon \approx -2t$. (e) The calculated DOS (black line) for $r = 0$ in (b). (f) The calculated DOS (black line) for $r = 1$ in (c). Red lines in (e) and (f) are the corresponding DOS calculated for concurrent charge modulations along a and b (i.e., such that $n' = n$) in which we assume $V_{x,0} = V_{y,0}$ (by no means a required constraint).

The splitting in Fig. 2(b) occurs concomitantly with an additional gap in the electronic density of states at $\varepsilon \approx -1.8t$ in Fig. 2(e) and a slightly weaker ordering gap at the Fermi energy ($\varepsilon_F \approx -t$) than in Fig. 2(f). A large V_x at $|k_y| \approx \frac{\pi}{4b}$ is therefore energetically unfavorable [29]. The momentum-dependent V_x (i.e., $r \approx 1$) avoids unfavorable splittings and gaps, moreover leaving the remaining open Fermi surfaces at $k_y \approx \pm\frac{\pi}{4b}$ amenable to a secondary Fermi surface instability of wave vector $\mathbf{Q}_y = [0, \frac{2\pi}{\lambda b}]$, which can further lower the density of states (and consequently the electronic energy) by forming a concurrent modulation along b [red line in Fig. 2(f)] [where $n' = n = 4$ in Eq. (1) in the case of bidirectional ordering]. By contrast, the splittings caused by a uniform potential (i.e., $r = 0$) mutually disrupt nesting for both $\mathbf{Q}_x$ and $\mathbf{Q}_y$ in the case of bidirectional ordering, leading to an energetically unfavorable higher density of states consisting of multiple peaks and valleys in the vicinity of the Fermi energy [red line in Fig. 2(e)].

On extending the bidirectional ordering density-of-states calculation to different periods in Fig. 3, we continue to find a well defined single gap with a broad deep minimum *only* in the case of momentum-dependent coupling [see Fig. 3(b)], pointing to its continuous evolution with λ. In the case of a uniform coupling [see Fig. 3(a)], by contrast, the multiple peaks and valleys vary discontinuously with λ.

Thus, by generating a deep wide gap in the density of states whose form and location in energy shifts continuously with λ, momentum-dependent coupling provides an incentive for incommensurate behavior in which λ adjusts itself in a continuous fashion so as to lower the electronic energy. Because the electronic energy in an itinerant picture is minimized by having the Fermi energy situated within a broad deep gap in the density of states, the λ-dependent gap provides an explanation for the evolution of the periodic structures seen in STM experiments as a function of doping [8]. The location of the minimum [identified by the dot-dashed line in Fig. 3(b)] enables us to estimate the hole doping p at which each period is most likely to be stable [plotted in Fig. 1(a)]. Using these dopings and assuming Luttinger's theorem [30], we calculate the corresponding Fermi surfaces in Fig. 4, whose forms consist of a single electron orbit (located close to the nodes) consistent with experimental observations [15,21]. Momentum-dependent coupling enables such a pocket to exist for weaker couplings than in Ref. [15] and to persist essentially unchanged as a function of doping. Most importantly, the near p-independent area [solid line in Fig. 1(b)] reproduces experimental observations (circles).

The subgaps occurring at the intersections of the electron orbits in Figs. 4(b) and 4(c) are small enough [$\Delta_{\text{sub}}^2/BF(\hbar e/m^*)^2 \ll 1$ provided $V_{x,y} \ll t_{10}$] to be completely broken down [31] in magnetic fields of the strength required to see magnetic quantum oscillations [9–11,16,17,21]—giving rise to a single orbit (thick magenta line) in strong magnetic fields. The subgaps nevertheless imply the absence of a simple (λ independent) relationship between the quantum oscillation frequency $F_e = (\hbar/2\pi e)A_e$ and the frequency $F_L = \frac{p}{2}F_{BZ}$ corresponding to the Luttinger hole doping (where $F_{BZ} = h/eab$ is the unreconstructed Brillouin zone

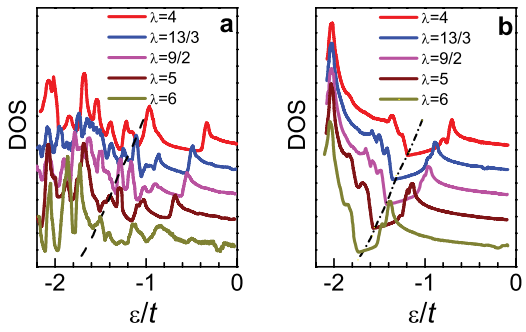

FIG. 3 (color online). (a) Electronic density-of-states (DOS) calculated for bidirectional charge modulations with periodicities corresponding to different multiples λ of the a and b lattice vectors as indicated, assuming uniform couplings $V_{x,0} = V_{y,0} = 0.3t$ in which $r = 0$. b Same as (b) but assuming momentum-dependent couplings in which $r = 1$ in Eq. (2). Curves have been offset for clarity. The dashed line in (b) indicates the minimum in the DOS near to which the Fermi energy is likely to be located.

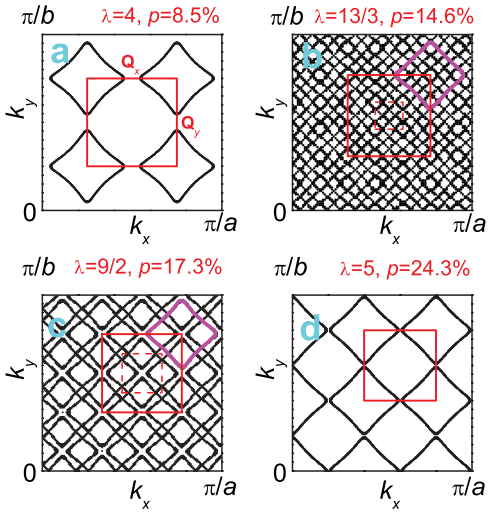

FIG. 4 (color online). (a), (b), (c) and (d) Reconstructed Fermi surface for selected λ's in Fig. 3(b) when the Fermi energy is situated at the minimum in the density-of-states, with the corresponding hole doping given. Solid red lines indicate the k-space area of the $\lambda a \times \lambda b$ superstructure, while dashed red lines indicate the n^2-fold reduced Brillouin zone [which coincides with the superstructure in (a) and (d)]. In (b) and (c), a magenta line is used to trace the path of the electronlike orbit that occurs in strong magnetic fields. $t_{10} \sim 100$ meV [23] produces an effective mass and gap consistent with experiments.

frequency). Only when the density-wave is "accidentally" commensurate such that subgaps do not occur (e.g., $\lambda = 4$ or 5) can adherence to Luttinger's theorem [30] be easily verified in quantum oscillation experiments. In Fig. 4(a), for example, $F_L = F_\lambda - F_e$ (where $F_\lambda = F_{BZ}/\lambda^2$ is the $\lambda a \times \lambda b$ superstructure frequency), while in Fig. 4(d) it is given by $F_L = \frac{7}{2}F_\lambda - F_e$.

Finally, we turn to aspects of momentum-selective density waves that may potentially be reconciled with the unidirectional behavior of charge ordering noted in the cuprates [7]. While closed Fermi surface pockets require modulations to occur concurrently along a and b lattice directions (in the absence of other orders [15]), the superposition of their ordering gaps in Fig. 2(f) (red line) implies the absence of a significant energy penalty (or interaction) associated with their interpenetration—in contrast to the uniform case in Fig. 2(e) where such a superposition does not occur. Given the implied independence of the modulations along a and b, underlying anisotropies in the electronic structure (such as that caused by the presence of chains in $YBa_2Cu_3O_{6+x}$ [24]) will likely produce anisotropies in $V_{x,y,0}$, λ, r and the onset temperature. In the present simulations, we find a Fermi surface consisting solely of an electron pocket to remain robust against an anisotropy $V_{x,0}/V_{y,0}$ as large as 4.

In conclusion, we present a model that explains the lack of a detectable doping-dependence of the quantum oscillation frequency in underdoped $YBa_2Cu_3O_{6+x}$ [i.e., Fig. 1(b) [20]]. By considering rational values of λ, we develop what is in essence an incommensurate model for cooperative charge- and bond-density-wave ordering in the cuprates [22,32]—here driven by a Fermi surface instability at the antinodes. By incorporating a (possibly dominant [29]) bond-density-wave component [22], the size of the periodic potential required to produce a single pocket with a small residual density-of-states is greatly reduced (i.e., $V_{x,y,0} \gtrsim 0.05t_{10}$) [29] relative to other models [13–15]. A key strength of the present model is its ability to reconcile doping-dependent quantum oscillation studies [16–21] with the doping-dependent λ seen in STM and other experiments [3,6,8] [i.e., Fig. 1(b)], the negative Hall and Seebeck coefficients over a broad range of dopings seen in transport [11] and particle-hole symmetry breaking reported at the antinodes in ARPES [2,12]—all while maintaining compliance with Luttinger's theorem [30].

The author acknowledges the DOE BES project "Science at 100 Tesla" and useful discussions with Ross McDonald and Arkady Shehter.

[1] P. A. Lee, N. Nagaosa, and X. G. Wen, Rev. Mod. Phys. **78**, 17 (2006).
[2] T. Kondo *et al.*, Nature (London) **457**, 296 (2009); R.-H. He *et al.*, Science **331**, 1579 (2011).
[3] X. Liu *et al.*, Phys. Rev. B **78**, 134526 (2008).
[4] S. B. Wilkins *et al.*, arXiv:1108.2444.
[5] J. E. Hoffman *et al.*, Science **295**, 466 (2002); T. Hanaguri *et al.*, Nature (London) **430**, 1001 (2004).
[6] T. Wu *et al.*, Nature (London) **477**, 191 (2011).
[7] S. A. Kivelson, Rev. Mod. Phys. **75**, 1201 (2003).
[8] W. D. Wise *et al.*, Nature Phys. **4**, 696 (2008).
[9] N. Doiron-Leyraud *et al.*, Nature (London) **447**, 565 (2007).
[10] E. A. Yelland *et al.*, Phys. Rev. Lett. **100**, 047003 (2008); A. F. Bangura *et al.*, Phys. Rev. Lett. **100**, 047004 (2008).
[11] D. LeBoeuf *et al.*, Nature (London) **450**, 533 (2007); F. Laliberté *et al.*, Nature Commun. **2**, 432 (2011).
[12] M. Hashimoto *et al.*, Nature Phys. **6**, 414 (2010).
[13] A. J. Millis and M. R. Norman, Phys. Rev. B **76**, 220503 (2007).
[14] S. Chakravarty and H. Y. Kee, Proc. Natl. Acad. Sci. U.S.A. **105**, 8835 (2008).
[15] N. Harrison and S. E. Sebastian, Phys. Rev. Lett. **106**, 226401 (2011).
[16] S. E. Sebastian *et al.*, Proc. Natl. Acad. Sci. U.S.A. **107**, 6175 (2010).
[17] B. Vignolle *et al.*, C.R. Physique **12**, 446 (2011).
[18] J. Singleton *et al.*, Phys. Rev. Lett. **104**, 86403 (2010).
[19] S. E. Sebastian, G. G. Lonzarich, and N. Harrison (unpublished).
[20] The scatter is related to small number of oscillations at some dopings. Upon close examination, the resistive oscillations of $YBa_2Cu_3O_{6+x}$ in Refs. [16,17,19,21] are seen to remain essentially in-phase for the range of dopings spanning $\approx 3\%$, implying that the same Landau level crosses the Fermi energy at the same field to within $\Delta B \sim 0.5$ T in all samples regardless of doping. From this we infer F to change by less than $(\Delta B/B)F \sim 5$ T (corresponding to $<1\%$ change in orbit area A_e).
[21] S. E. Sebastian *et al.*, Nature Commun. **2**, 471 (2011).
[22] C. Nayak, Phys. Rev. B **62**, 4880 (2000).
[23] We use $\varepsilon = \varepsilon_0 + 2t_{10}[\cos ak_x + \cos bk_y] + 2t_{11}[\cos(ak_x + bk_y) + \cos(ak_x - bk_y)] + 2t_{20}[\cos 2ak_x + \cos 2bk_y]$ [24], with $t_{11}/t_{10} = -0.5$ and $t_{20}/t_{10} = 0.1$ chosen to reproduce the $YBa_2Cu_3O_{6+x}$ Fermi surface from recent ARPES [25].
[24] O. K. Andersen *et al.*, Phys. Chem. Solids **56**, 1573 (1995).
[25] Y. Sassa *et al.*, Phys. Rev. B **83**, 140511 (2011).
[26] V. Brouet *et al.*, Phys. Rev. B **77**, 235104 (2008).
[27] K. Rossnagel, J. Phys. Condens. Matter **23**, 213001 (2011).
[28] The k-dependent matrix elements in Eq. (1) become $V_x(\mathbf{k} + i\mathbf{Q}_y)$ and $V_y(\mathbf{k} + j\mathbf{Q}_x)$ where i and j refer to the multiples of $\mathbf{Q}_y$ and $\mathbf{Q}_x$ by which ε is translated. Since the primary function of the k dependence is to inhibit splitting of the open sheets in Fig. 2, we neglect the k_x dependence of V_x and the k_y dependence of V_y.
[29] r-dependent calculations reveal the DOS and free energy to be lowest when $r = 1.35$ (considering $\lambda = 4$) for the Fermi surface considered, implying a dominant bond-density-wave component (with V_x and V_y exhibiting nodes at $k_y = \frac{\pi}{b} \pm \frac{|\mathbf{Q}_y|}{2}$ and $k_x = \frac{\pi}{a} \pm \frac{|\mathbf{Q}_x|}{2}$ respectively).
[30] J. M. Luttinger, Phys. Rev. **119**, 1153 (1960).
[31] E. Fawcett, Rev. Mod. Phys. **60**, 209 (1988).
[32] S. Sachdev, Rev. Mod. Phys. **75**, 913 (2003).